




Whole brain volume and cortical thickness abnormalities in Wilson's disease: a clinical correlation study

Yukun Song¹ · Lin Zou² · Jing Zhao³ · Xiangxue Zhou⁴ · Yingqian Huang³ · Haishan Qiu³ · Haiwei Han¹ · Zhiyun Yang³ · Xunhua Li⁴ · Xiaoying Tang² · Jianping Chu³ 

© Springer Science+Business Media, LLC, part of Springer Nature 2020

Abstract

Wilson's disease (WD) is an inherited autosomal recessive disorder of copper metabolism, and its neurological and neuropsychiatric manifestations are associated with copper accumulation in brain. A few neuroimaging studies have shown that gray matter atrophy in WD affects both subcortical structures and cortex. This study aims to quantitatively evaluate the morphometric brain abnormalities in patients with WD in terms of whole brain volume and cortical thickness and their associations with clinical severity of WD. Thirty patients clinically diagnosed as WD with neurological manifestations and 25 healthy controls (HC) were recruited. 3D T1-weighted images were segmented into 276 whole-brain regions of interest (ROIs) and 68 cortical ROIs. WD-vs-HC group comparisons were then conducted for each ROI. The associations between those morphometric measurements and the Global Assessment Scale (GAS) score for WD were analyzed. Compared with HC, significant WD-related volumetric decreases were found in the bilateral subcortical nuclei (putamen, globus pallidus, caudate nucleus, substantia nigra, red nucleus and thalamus), diffuse white matter and several gray matter regions. WD patients showed reduced cortical thickness in the left precentral gyrus and the left insula. Further, the volumes of the right globus pallidus, bilateral putamen, right external capsule and left superior longitudinal fasciculus were negatively correlated with GAS. Our results indicated that significant WD-related morphometric abnormalities were quantified in terms of whole-brain volumes and cortical thicknesses, some of which correlated significantly to the clinical severity of WD. Those morphometrics may provide a potentially effective biomarker of WD.

Keywords Wilson's disease · Structural MRI · Whole brain volume · Cortical thickness

Introduction

Wilson's disease (WD) is an inherited autosomal recessive disorder of copper metabolism leading to copper accumulation in hepatocytes and extrahepatic organs (Ala et al. 2007; Członkowska et al. 2018). While neurological and neuropsychiatric manifestations related to WD are classically associated with copper accumulation in brain (Bandmann et al. 2015).

During the past several years, there have been a very few quantitative researches on WD-related brain abnormalities using advanced neuroimaging techniques. Two voxel-based morphometry (VBM) studies have demonstrated that the volumes of grey matter (GM) in the frontal, occipital and temporal lobes, basal ganglia, cerebellum and thalamus were decreased in WD patients (Hu et al. 2017; Stezin et al. 2016). However, VBM has been shown to be sensitive to whole brain image registration errors (Ashburner 2009), especially in cortical regions wherein the topology varies hugely from subject to subject. It is challenging to distinguish whether the

Yukun Song and Lin Zou contributed equally to this work.

✉ Xiaoying Tang
tangxy@sustech.edu.cn

✉ Jianping Chu
chujping@mail.sysu.edu.cn

¹ Department of Radiology, The First Affiliated Hospital of Xiamen University, Xiamen 361001, Fujian Province, China

² Department of Electrical and Electronic Engineering, Southern University of Science and Technology, Shenzhen 518052, Guangdong Province, China

³ Department of Radiology, The First Affiliated Hospital of Sun Yat-sen University, Guangzhou 510080, Guangdong Province, China

⁴ Department of Neurology, The First Affiliated Hospital of Sun Yat-sen University, Guangzhou 510080, Guangdong Province, China

abnormality patterns identified from VBM are real or just noises induced by the inaccurate image registration.

As an alternative to VBM, whole brain segmentation based on volumetric analysis has been applied, which is more intuitive and more robust. Volumetric analysis in this study was conducted by using a multi-atlas pipeline built upon a two-level Bayesian parameter estimation algorithm called the Multi-Atlas Likelihood Fusion (MALF) algorithm (Tang et al. 2013; Wang et al. 2013) which overcomes the shortness of VBM analysis method (or has a higher accuracy in calculating the brain volume and cortical thickness). Whole brain segmentation has been applied to a variety of brain disease analyses, such as Alzheimer's disease and Parkinson's disease (Liu et al. 2019; Chen et al. 2017; Kamagata et al. 2017), but not WD. In addition to whole brain volumes, cortical thicknesses are also important brain morphometrics to investigate (Fischl et al. 2004). However, no quantitative MRI study has been performed for the investigation of cortical thickness abnormality patterns in WD.

Although WD was first described more than a century ago, the exact changes of volume and cortical thickness in the whole brain about how WD will affect brain are far from clear. And there have been a very few quantitative researches on WD-related brain abnormalities using advanced neuroimaging techniques during the past several years. Our purpose of this study is to focus on the new techniques and to explore their utility in WD. We hope this study can offer a priori for the further whole brain analyses in WD and further explore the imaging biomarkers to assess disease progression. In this study, we hypothesize that there are whole brain volume abnormalities, including GM and white matter (WM), and cortical thickness abnormalities in the pathology of WD and the identified morphometric abnormalities significantly correlate with clinical severity of WD.

Methods

Subjects

Thirty patients with WD (18 males, 12 females, mean age: 27.93 ± 5.37 years, range: 18–37 years) at an untreated stage with neurological manifestations as confirmed by clinical and laboratory examinations, and 25 healthy controls (HC, 15 males, 10 females, mean age: 28.12 ± 5.62 years, range: 18–38 years) with age, gender and years of education matched were enrolled in this study. All subjects were right-handed and underwent a series of neurological tests, including the Global Assessment Scale for WD (GAS for WD) (Aggarwal et al. 2009), the Mini-Mental State Examination (MMSE) (Tombaugh and McIntyre 1992), the Hamilton Depression Rating Scale (HAM-D) (Hamilton 1960) and the Hamilton Anxiety Rating Scale (HAM-A) (Hamilton 1959). Diagnostic criteria (Ferenci et al. 2003) of

WD include a ceruloplasmin concentration less than 0.2 g/L, a 24-h urinary copper excretion greater than 100 μg , the presence of K-F rings on slit-lamp examination and clinical symptoms (such as the presentation of extrapyramidal symptoms and signs, with dysarthria and tremor, and remarkable impairment of liver function). Two experienced neurologists scored each patient's clinical symptoms by GAS. The disease duration time of each patient, from the time of disease onset (self-reported) to the time of MRI scanning, was recorded. None of the patients had a history of neurological diseases other than WD. For HC, all participants were enrolled from college students or society officers and those who failed to meet the following research criteria points were excluded: (a) without central nervous system diseases, mental diseases, nor other serious diseases; (b) the MMSE, HAM-D and HAM-A scores within the normal range (adjusted for age, sex, and education); and (c) a GAS score of 0. Table 1 summarized the clinical and demographic characteristics of all subjects. This study was approved by the Medical Ethical Committee of The First Affiliated Hospital of Sun Yat-sen University. Informed consent was obtained from all participants.

MRI data acquisition

All MRI scans were performed on a 3.0 T MRI scanner (Magnetom Trio, Siemens Healthcare, Erlangen, German), using a 12-channel head coil. For each participant, the T1-weighted brain image was acquired using a 3D magnetization prepared-rapid acquisition gradient echo (MP-Rage) sequence. Scanning parameters are shown as follows: TR = 1750 ms, TE = 2.88 ms, TI = 900 ms, matrix = 384×384 , FOV = $260 \text{ mm} \times 260 \text{ mm}$, voxel size = $0.7 \text{ mm} \times 0.7 \text{ mm} \times 0.7 \text{ mm}$ (256 slices and without slice gap), flip angle = 9° , and the acquisition time was 4.21 min. All MRI images were visually inspected by one experienced neurologist and one neuroradiologist.

Whole-brain volumetric segmentation

A multi-atlas pipeline (a module implemented at www.mricloud.org) was used to segment T1-weighted images into a total of 276 whole-brain anatomical ROIs. In the current study, we used 45 atlases (available at the MriCloud website) which are in a similar age range as that of our 55 participants. Details of the selected atlas set, and their label definitions have been described elsewhere (Mori et al. 2016). All segmentation results were examined visually and verified repeatedly to guarantee the accuracy of each segmentation. Then the volumetric measurement of each ROI was calculated as the total number of voxels within the corresponding ROI multiplied by the voxel resolutions ($0.7 \text{ mm} \times 0.7 \text{ mm} \times 0.7 \text{ mm}$). The volume decrease rate of a structure was defined as $(V_{HC} - V_{WD}) / V_{HC} \times 100\%$, with V representing the average volume of a specific group.

Table 1 Clinical and demographic characteristics of all subjects enrolled in this study

Characteristics	WD (<i>N</i> = 30)	HC (<i>N</i> = 25)	<i>P</i> ^a values
Gender (male/female)	18/12	15/10	0.608
Age (years)	27.93 ± 5.37	28.12 ± 5.62	0.900
Education (years)	13.10 ± 2.23	13.84 ± 2.69	0.270
Handedness (right/left)	30/0	25/0	—
Disease duration (months)	43.87 ± 19.51	—	—
WD types	neurologic	—	—
Family history	100.00%	—	—
KF ring present	100.00%	—	—
24 h urinary copper excretion (μg)	785.80 ± 424.91	—	—
Ceruloplasmin (g/L)	0.64 ± 0.40	—	—
GAS score for WD	15.64 ± 6.64	0.00 ± 0.00	—
MMSE score			
Mean (SD)	28.30 ± 2.51	29.12 ± 1.09	0.133
<i>N</i> % ^b	86.67%	100.00%	0.135
HAMD score			
Mean (SD)	10.90 ± 5.71	1.88 ± 2.20	< 0.001
<i>N</i> % ^b	40.00%	100.00%	< 0.001
HAM-A score			
Mean (SD)	13.93 ± 7.35	1.32 ± 1.70	< 0.001
<i>N</i> % ^b	16.67%	100.00%	< 0.001

Data are mean ± standard deviation. Statistical significance was set to $P < 0.05$

Normal reference range: 24 h urinary copper excretion, 15–30 μg; Ceruloplasmin, 0.2–0.4 g/L; MMSE score, ≥23 for high school education and ≥24 for college education; HAMD score, 0–8; HAM-A score, 0–7

WD Wilson's disease, HC Healthy controls, *N* Number, KF Kayser-Fleischer; —, Not available, MMSE Mini-Mental State Examination

^a *P* values for continuous variables derived from Student's *t* test; categorical variables from Chi-square test

^b Proportion of normal subjects

Surface-based cortical thickness measurement

Surface-based cortical thickness measurements for 68 cortical ROIs were automatically obtained from the FreeSurfer software (version 5.0). The surface-based stream comprised in the FreeSurfer analysis pipeline includes some preliminary steps as follows: motion correction, affine registration to Talairach atlas, intensity normalization, skull stripping, automatic sub-cortical segmentation including neck removal (Desikan et al. 2006; Fischl et al. 2004), segmentation of WM and GM structures (<http://surfer.nmr.mgh.harvard.edu/fswiki>) and so on. After that, the mid brain is cut from the cerebrum and the hemispheres are separated from each other in step Cut/Fill. The subsequent steps involve tessellation of GM-WM boundary (Dale et al. 1999), original surface smoothing, inflation for minimize metric distortion, automatic topology correction, and surface formation in which the GM-WM boundary and pial surface are estimated and optimized. The shortest distance between the pial surface and the GM-WM boundary at each vertex across the cortical mantle was calculated as the value of the cortical thickness. Estimated total intracranial volume

(eTIV) and cortical thickness were respectively extracted from the aseg.stats and lh/rh.aparc.stats file, which are part of the results obtained from the “recon-all” batch command.

For cortical thickness estimation and analysis, all data were processed using the same version of FreeSurfer software, the details of which have been described elsewhere (Fischl and Dale 2000; Fischl et al. 1999). It should be noted that no manual correction was made to any of the FreeSurfer results to ensure a valid analysis. However, a visual inspection was conducted to check the quality of the FreeSurfer results.

Group comparison analysis

To assess whether there is any significant WD-vs-HC difference in each volume measurement and each cortical thickness measurement, inner-group comparisons were conducted using a linear regression model (Tang et al. 2014), namely $J_k(s)$

$= \alpha_k + \beta_k Y(s) + \sum_{cov} \alpha_{cov} X_{cov}(s) + \varepsilon_k(s)$, where $J_k(s)$ denotes a specific measurement (volume or cortical thickness) of specific structures of interest k for subject

s , $X_{\text{cov}}(s)$ represents the covariate information of participants (for this study, eTIV, age, gender and years of education were used as covariates), $\varepsilon_k(s)$ denotes a Gaussian noise structure $N(0, \sigma_k^2)$ and $Y(s)$ is a binary group variable (0 for HC, and 1 for WD). We tested the null hypothesis $H_0: \beta_k = 0$ against the general hypothesis $H_0: \beta_k \neq 0$ simultaneously for all volume measurements and all cortical thicknesses. The statistical significance of each group comparison was quantified using a P value from Fisher's method of randomization. In both the whole-brain volumetric analysis and the cortical thickness analysis, multiple comparison correction was carried out by controlling the familywise error rate (FWER) at a level of 0.05 based on the maximum statistic method. Accordingly, a two side of P value < 0.05 is considered statistical significance in the volumetric analysis, and a two side of P value < 0.0013 is considered statistical significance in the cortical thickness analysis.

Statistical analysis

Statistical analyses were performed with R (Version 3.3.2 for Windows, Comprehensive R Archive Network, <http://cran.r-project.org>). The Shapiro-Wilk test was used for analysis of normal distribution; demographic and clinical data were analyzed by Student's t test for continuous variables and the χ^2 test for categorical variables. Pearson correlation coefficient analysis was used to assess the correlation between each morphometric measurement (volume and cortical thickness) and the GAS score, MMSE score, HAMD score, HAM-A score, disease duration, 24 h urinary copper excretion, and ceruloplasmin. The significance level was set to be 0.05. Multiple comparison correction by controlling the FWER at a level of 0.05 was conducted in the correlation analysis, resulting in a two side of P value < 0.0025 is considered statistical significance.

Results

Whole-brain volume analysis

After FWER correction, significant WD-related volumetric decreases were found in the subcortical nuclei, including the bilateral putamen, globus pallidus, caudate nucleus, substantia nigra, red nucleus and thalamus ($P < 0.0001$). Diffuse WM regions and some GM regions (bilateral cingulate gyrus and bilateral superior frontal gyrus) were also found to have significant volumetric decreases in the WD group. In addition, significant volumetric increases were found in the lateral ventricle, the third ventricle, the sylvian fissure and insular sulcus ($P < 0.0001$) (Fig. 1). More details regarding the whole-brain volumetric differences between the two groups are presented in the Appendices Table 3.

In terms of the volume change rate, we found that the bilateral superior fronto-occipital fasciculus (right: 53.29%, left: 44.59%), putamen (right: 48.32%, left: 47.15%), external capsule in the claustrum (right: 37.52%, left: 42.88%), substantia nigra (right: 38.24%, left: 35.09%), left globus pallidus (37.13%) and left nucleus accumbens (34.66%) were the top ten structures exhibiting the highest volume change rates. For detailed results, please see the Appendices Table 3.

Cortical thickness analysis

After FWER correction, patients with WD showed decreased mean cortical thickness in the left precentral gyrus and the left insula ($P < 0.0013$), as shown in Fig. 2 and Table 2. There were no significant differences in the eTIV and cortical thickness of other structures in patients with WD.

Correlation analysis

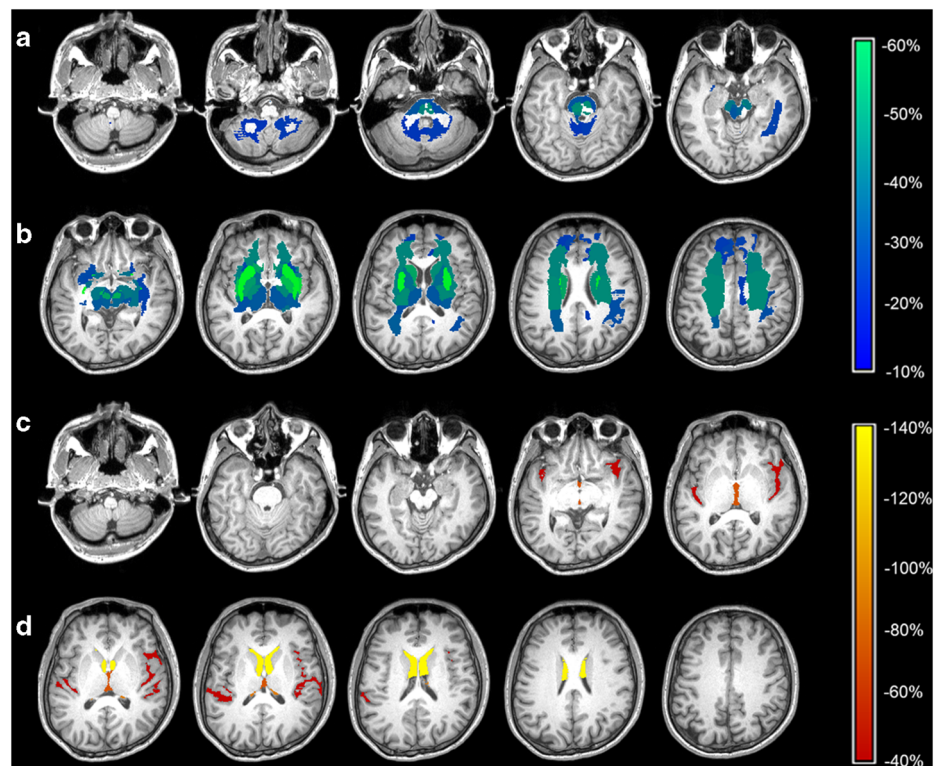
For the whole-brain volumetric measurements, statistically significant correlations to the GAS score were found in the left putamen ($r = -0.691$, $P < 0.001$) and right putamen ($r = -0.729$, $P < 0.001$), in the WD group, after FWER correction at a threshold of $P = 0.0025$ (Fig. 3). No significant correlations were found between other clinical characteristics and volume measurements. No significant correlations were found among the GAS score, MMSE score, HAMD score, HAM-A score, disease duration, 24 h urinary copper excretion, ceruloplasmin and any of the 68 cortical thicknesses in patients with WD.

Discussion

In the present study, we quantitatively investigated WD-related abnormality patterns of the volumes of 276 whole-brain ROIs and cortical thicknesses of 68 cortical ROIs. Our study yielded three findings: Firstly, volumetric analysis demonstrated significant atrophy of various brain structures and significant expansion of the ventricular system in patients with WD. The brain atrophy was prominent in the basal ganglia, especially the lenticular nucleus (globus pallidus and putamen). Secondly, cortical thickness analysis showed that patients with WD were characterized by cortical thinning in the left precentral gyrus and the left insula. Finally, the volumes of bilateral putamen were significantly correlated with clinical severity in patients with WD.

In agreement with previous neuroimaging studies in Wilson's disease (Li et al. 2018; Stezin et al. 2016; Zou et al. 2019), we observed similar structural changes in the basal ganglia, cerebellum, midbrain, pons, diffuse WM regions and some GM regions in our patients. These signal changes are reported to be due to edema, neuronal necrosis,

Fig. 1 Volumetric comparison results between WD and HC groups. Fig (a, b): Maps of whole brain atrophy patterns. Fig. (c, d): Maps of whole brain expansion patterns. The color bar denotes the volume decrease rate (%) at regions that had survived the FWER correction



gliosis, demyelination, or cystic degeneration of neurons due to copper overload, which leading to the atrophy of the corresponding structures and then causing the corresponding clinical symptoms (Członkowska et al. 2018; Kalita et al. 2017).

It is known that the basal ganglia are important components of the extrapyramidal system (Bostan and Strick 2018). The main function of the basal ganglia is to control and adjust limb movements. In this study, the abnormal atrophy observed in

the basal ganglia might be the cause of limb movement-related disorders in WD. It has been proved by many studies (Ala et al. 2007; Członkowska et al. 2018; Rodriguez-Castro 2015) that copper mainly deposits in the basal ganglia of WD, which are actively involved in the coordination of movement. Our findings showed that the brain atrophy was prominent in the globus pallidus and putamen. This result is consistent with previous histological and clinical studies.

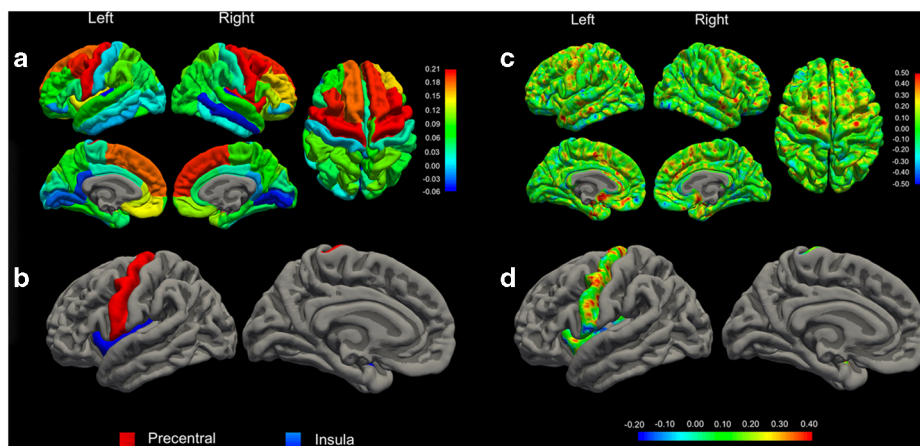


Fig. 2 Cortical thickness comparison results between WD and HC groups. Fig (a, b): Maps of the mean cortical thickness group differences at different brain lobes. Fig. (c, d): Maps of the vertex-wise cortical thickness group differences at different brain lobes. The color bar denotes the group difference of mean values (mm) at regions that had survived the FWER correction. Warmer color denotes regions where

cortical thickness is greater in HC, and cooler color denotes regions where WD patients have greater cortical thickness. Fig. (a, c): significant group differences, $P < 0.05$ uncorrected for multiple comparisons. Fig. (b, d): significant group differences, $P < 0.0013$ corrected for multiple comparisons. Fig. (d) shows that some areas of left precentral gyrus and left insula have decreased cortical thickness by approximately 5 mm (red)

Table 2 Mean cortical thickness (mm) of cortical ROIs exhibiting significant WD-vs-HC group differences

Structure	HC (mm)	WD (mm)	P values
WD < HC			
Caudal middle frontal (left)	2.59 ± 0.02	2.39 ± 0.06	0.0016
Medial orbitofrontal (left)	2.63 ± 0.01	2.49 ± 0.04	0.0251
Precentral (left)	2.53 ± 0.02	2.32 ± 0.04	0.0001
Superior frontal (left)	2.87 ± 0.01	2.69 ± 0.05	0.0193
Superior parietal (left)	2.19 ± 0.01	2.09 ± 0.02	0.0072
Supramarginal (left)	2.52 ± 0.02	2.42 ± 0.03	0.0225
Insula (left)	3.05 ± 0.02	2.91 ± 0.04	0.0004
Caudal middle frontal (right)	2.57 ± 0.01	2.38 ± 0.06	0.0300
Paracentral (right)	2.43 ± 0.03	2.34 ± 0.04	0.0350
Precentral (right)	2.49 ± 0.02	2.3 ± 0.06	0.0091
Precuneus (right)	2.38 ± 0.01	2.31 ± 0.02	0.0353
Rostral middle frontal (right)	2.43 ± 0.01	2.29 ± 0.03	0.0144
Superior frontal (right)	2.84 ± 0.01	2.66 ± 0.04	0.0153
Superior parietal (right)	2.17 ± 0.01	2.07 ± 0.02	0.0267
Insula (right)	3.13 ± 0.01	2.94 ± 0.07	0.0041
WD > HC			
Lingual (left)	1.92 ± 0.01	1.95 ± 0.02	0.0452
Lingual (right)	1.96 ± 0.01	1.99 ± 0.02	0.0210

Data are expressed as mean ± standard deviation

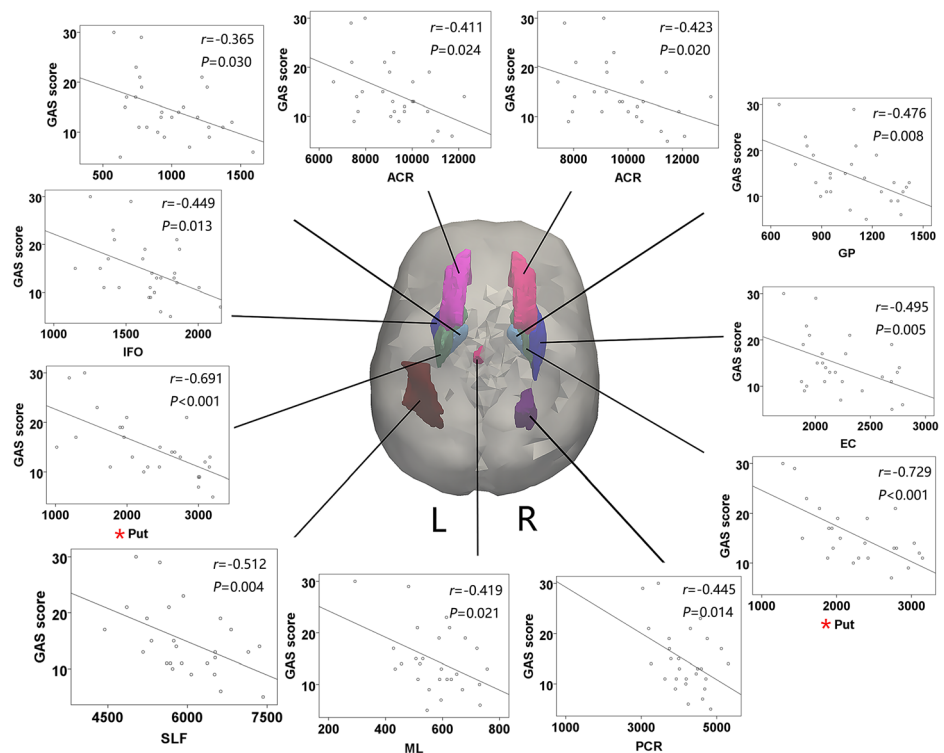
Regular: results significant ($P < 0.05$) without correction for multiple comparisons; Bold: results significant with FWER correction ($P < 0.0031$)

HC Healthy controls, WD Wilson's disease

As for the cortical abnormalities in WD, Hu et al. (Hu et al. 2017) found GM volume decreases in the middle and medial frontal gyrus, superior and middle occipital gyrus, precentral and paracentral lobule, from a VBM analysis. Stezin et al. (Stezin et al. 2016) also used VBM to reveal a significant GM volume loss in the temporal gyrus, frontal gyrus, precentral gyrus and supramarginal gyrus. VBM can only reflect cortical volume patterns but not cortical thickness patterns. Our complementary volume and thickness analyses showed GM volume decreases in the left cingulate gyrus and the bilateral superior frontal gyrus, but cortical thinning in the left precentral gyrus and the left insula. These results may suggest that volume and cortical thickness are measures at different dimensions, so the WD-related GM morphometric abnormalities have different patterns in terms of 3D volume and 2D cortical surface.

The precentral gyrus and superior frontal gyrus are related to memory processing, self-relevant processes and motor function (Guo et al. 2018; Li et al. 2013). Cortical atrophy in these regions may be associated with behavioural, cognitive and motor dysfunctions in patients with WD. Insula and cingulate gyrus are part of the limbic system, which plays an important role in emotion, behavior, motivation, self-awareness, cognitive function and interpersonal experience (Zhang et al. 2019; Caruana et al. 2018). Some patients with WD can behave as mental disorders, including anxiety, depression and excitement, etc. The mental symptoms of these patients may be related to the atrophy of the Insula and cingulate gyrus. This may also account for the difference in emotional scale scores between HC and WD.

Fig. 3 Regions where volumes significantly correlated with the GAS score in the WD group. * Significant correlation corrected for FWER correction ($P < 0.0025$). Volumes of the right putamen show the strongest correlation with GAS score. GAS, Global Assessment Scale for WD; L, left; R, right; ACR, anterior corona radiata; GP, globus pallidus; EC, external capsule; Put, putamen; PCR, posterior corona radiata; ML, medial lemniscus; SLF, superior longitudinal fasciculus; IFO, inferior fronto-occipital fasciculus



In addition to GM atrophy, our study also found diffuse WM atrophy in WD, and the superior fronto-occipital fasciculus showed the most significant atrophy. It is known that WM lesions in WD showed obvious tissue sparsity and cavity, and the WM fibers of the internal and external capsules showed multiple demyelination (Członkowska et al. 2018; Lorincz 2018). These pathological changes may result in decreases in the volumes of the corresponding structures. Jadav et al. (Jadav et al. 2013) employed diffusion tensor imaging (DTI) to analyze patients with WD and found WM damages of the internal capsule, midbrain, pons, frontal and occipital lobes. This may suggest that WM degeneration could also present in WD.

Pearson correlation analysis showed a negative correlation between clinical score and the volumes of bilateral putamen in patients with WD, indicating that the severity of neurological symptoms may be related to nuclei of basal ganglia which are easily injured by copper deposition. The right putamen was one of the most prominently involved structures and its volume loss showed a most significant correlation with clinical scores. And thus, the right putamen volume may serve as an imaging biomarker for assessing the progression of clinical severity and the efficiency of decoppering therapy. To be noted, our study included 30 young patients with a limited sample size and a relatively short clinical course, which may explain that no correlation was found between cortical thicknesses measurements and the clinical features in patients with WD.

Previous studies were most based on VBM method, which were mainly focused on subcortical structures and cortex, but not the whole brain. In contrast, our data analyzed the whole brain volumes of 276 ROIs and cortical thicknesses of 68 cortical ROIs. ROI approach is another useful method to analyze whole brain structures. It allows for direct and accurate examination of the way that disease progression patterns take effect on specific structures of interest. In addition, VBM can only reflect cortical volume patterns, while our complementary surface-based analysis suggested that the WD-related GM morphometric abnormalities have different patterns in terms of cortical thickness. Besides methodological differences, we think, due to various reasons such as different study samples, different durations of disease and whether patients were in untreated stages, there may produce differences in different researches.

There are still several limitations of this study. First, our sample size is kind of limited. Second, our study did not classify the disease according to the disease duration and neurological symptoms due to the limited sample size. As such, our future research plans are to enlarge the sample size and update our findings.

Conclusions

In conclusion, this study quantitatively evaluated the brain atrophy patterns of WD and demonstrated morphological

abnormalities in whole brain volumes and cortical thicknesses. The identified neuroimaging abnormalities in WD can improve our understanding of the pathogenesis and progression of the disease. Moreover, certain morphometric characteristics, such as the volumes of several WM regions and the basal ganglia nuclei, maybe used as an imaging biomarker to assess disease progression.

Acknowledgements We thank Zhuoyi Peng, Xinbei Li, Yuliang Wang, and Yisu Tian for their research assistance, and all participants involved in this study.

Author contributions Conception and study design (SYK, CJP and TXY), data collection or acquisition (SYK, ZL, HXQ, QHS and ZJ), statistical analysis (SYK, ZL), interpretation of results (SYK, ZL, HYQ, QHS, TXY and CJP), drafting the manuscript work or revising it critically for important intellectual content (SYK, ZL, TXY and CJP) and approval of final version to be published and agreement to be accountable for the integrity and accuracy of all aspects of the work (All authors).

Funding This work was supported by the National Key R&D Program of China (2017YFC0112404), the National Natural Science Foundation of China (NSFC 81501546 and NSFC 81201074), and the Science and Technology Program of Guangdong Province (201508020121) and the Natural Science Foundation of Guangdong Province (2017A030313676).

Compliance with ethical standards

Conflict of interests None of the authors have a conflict of interest to declare.

Ethical approval All procedures performed in studies involving human participants were in accordance with the ethical standards of the institutional and/or national research committee and with the 1964 Helsinki declaration and its later amendments or comparable ethical standards.

Informed consent Informed consent was obtained from all individual participants included in the study.

Appendices

Subjects

There were significant group differences in HAMD score (WD: 10.90 ± 5.71 , HC: 1.88 ± 2.20) and HAM-A score (WD: 13.93 ± 7.35 , HC: 1.32 ± 1.70) between WD and HC ($P < 0.05$). No significant differences were found in gender ($P = 0.608$, χ^2 test), age ($P = 0.900$, Student's t test), years of education ($P = 0.270$, Student's t test) nor MMSE score ($P = 0.133$ for Student's t test, $P = 0.135$ for χ^2 test) between WD and HC. For the patients with WD, the mean total disease duration time was 43.87 ± 19.51 months (range: 12–84 months) and the mean GAS score was 15.64 ± 6.64 (range: 5–30). A higher GAS score indicates a more severe clinical symptom. (Table 1)

Table 3 Mean volumes (mm³) of whole brain ROIs showing significant WD-vs-HC group differences

Structure	HC	WD	Volume decrease rate	P values
Abbreviation	full name			
WD < HC				
SFO R	superior fronto-occipital fasciculus (right)	202.96 ± 41.28	94.81 ± 36.41	53.29%
Put R	putamen (right)	4644.45 ± 479.54	2393.89 ± 637.93	48.32%
Put L	putamen (left)	4526.80 ± 480.30	2378.78 ± 750.87	47.15%
SFO L	superior fronto-occipital fasciculus (left)	297.00 ± 54.03	164.56 ± 60.18	44.59%
ECCL L	external capsule in the claustrum (left)	484.79 ± 52.73	276.93 ± 72.34	42.88%
Snigra L	substantia nigra (left)	398.70 ± 34.50	213.94 ± 78.05	38.24%
ECCL R	external capsule in the claustrum (right)	525.58 ± 55.58	328.37 ± 65.41	37.52%
GP L	globus pallidus (left)	1527.86 ± 189.00	987.11 ± 289.23	37.13%
Snigra R	substantia nigra (right)	268.38 ± 45.60	185.20 ± 45.35	35.09%
NucAccumbens L	nucleus accumbens (left)	700.75 ± 60.38	457.89 ± 116.64	34.66%
RedNc L	red nucleus (left)	289.14 ± 41.90	197.78 ± 27.58	34.46%
Caud R	caudate nucleus (right)	3502.58 ± 409.96	2374.7 ± 433.66	32.20%
RedNc R	red nucleus (right)	312.42 ± 35.85	221.70 ± 62.35	31.89%
NucAccumbens R	nucleus accumbens (right)	815.54 ± 82.64	559.89 ± 123.41	31.35%
GP R	globus pallidus (right)	1578.98 ± 188.23	1096.85 ± 233.21	30.59%
subgenualWM ACC R	subcortical white matter of the subgenual anterior cingulate cortex (right)	93.25 ± 18.34	64.78 ± 15.03	30.53%
subgenualWM ACC L	subcortical white matter of the subgenual anterior cingulate cortex (left)	200.25 ± 31.11	142.11 ± 29.62	29.03%
PCT R	pontine crossing tract (right)	582.50 ± 81.82	416.59 ± 81.79	28.48%
CST L	corticospinal tract(left)	1453.58 ± 195.59	1044.70 ± 222.37	28.13%
PLIC R	posterior limb of internal capsule (right)	2973.54 ± 269.37	2148.11 ± 406.86	27.76%
Caud L	caudate nucleus (left)	3489.04 ± 399.55	2529.52 ± 778.43	27.50%
SCR R	superior corona radiata (right)	15,170.83 ± 1653.43	11,036.81 ± 1558.27	27.25%
CST R	corticospinal tract(right)	1258.17 ± 124.26	915.96 ± 182.90	27.20%
SCR L	superior corona radiata (left)	15,428.67 ± 1707.53	11,259.37 ± 1718.77	27.02%
ML L	medial lemniscus (left)	789.42 ± 92.91	576.70 ± 107.65	26.95%
PLIC L	posterior limb of internal capsule (left)	2927.29 ± 249.74	2142.37 ± 401.62	26.81%
ACR R	anterior corona radiata (right)	13,192.63 ± 1425.59	9768.41 ± 1473.60	25.96%
EC L	external capsule (left)	2986.21 ± 235.91	2217.41 ± 294.36	25.75%
ACR L	anterior corona radiata (left)	12,397.46 ± 1277.73	9240.81 ± 1437.56	25.46%
ML R	medial lemniscus (right)	962.42 ± 119.31	720.85 ± 112.27	25.10%
EC R	external capsule (right)	2969.96 ± 217.33	2232.00 ± 327.81	24.85%
CP L	cerebral peduncle (left)	1876.92 ± 188.51	1434.19 ± 279.67	23.59%
CP R	cerebral peduncle (right)	1976.04 ± 198.72	1513.52 ± 250.70	23.41%
Fx/ST L	fornix/stria terminalis (left)	1464.08 ± 131.08	1133.22 ± 136.64	22.60%
BasalForebrain L	basal forebrain (left)	1785.13 ± 155.22	1393.04 ± 151.01	21.96%
ALIC R	anterior limb of internal capsule (right)	2189.42 ± 248.78	1716.78 ± 277.87	21.59%
BasalForebrain R	basal forebrain (right)	1577.96 ± 155.84	1245.15 ± 138.66	21.09%
ALIC L	anterior limb of internal capsule (left)	2143.29 ± 207.18	1697.07 ± 307.27	20.82%
Midbrain L	midbrain (left)	2348.92 ± 207.39	1877.48 ± 322.73	20.07%
Midbrain R	midbrain (right)	2313.29 ± 192.35	1888.7 ± 281.50	18.35%
PCR R	posterior corona radiata (right)	5102.92 ± 720.25	4175.22 ± 583.08	18.18%
RLIC L	retrolenticular part of internal capsule (left)	2900.63 ± 294.63	2385.11 ± 317.16	17.77%

Table 3 (continued)

Structure	full name	HC	WD	Volume decrease rate	P values
Thalamus R	thalamus (right)	6128.18 ± 753.20	5080.11 ± 759.68	17.20%	<0.0001
MCP R	middle cerebellar peduncle (right)	3053.50 ± 366.10	2545.74 ± 337.98	16.63%	0.0002
Thalamus L	thalamus (left)	5877.66 ± 424.71	4880.59 ± 784.86	16.58%	<0.0001
SCP R	superior cerebellar peduncle (right)	864.25 ± 87.07	722.19 ± 92.77	16.44%	<0.0001
RLIC R	retrolenticular part of internal capsule (right)	2955.33 ± 290.84	2494.93 ± 324.88	15.58%	<0.0001
SILF L	superior longitudinal fasciculus (left)	7134.71 ± 840.30	6052.41 ± 840.49	15.17%	<0.0001
MCP L	middle cerebellar peduncle (left)	2797.79 ± 303.53	2381.81 ± 309.24	14.87%	0.0001
IFO R	inferior fronto-occipital fasciculus (right)	2035.71 ± 151.09	1741.04 ± 206.92	14.48%	<0.0001
CI R	claustrum (right)	469.38 ± 37.13	404.89 ± 48.78	13.74%	<0.0001
IFO L	inferior fronto-occipital fasciculus (left)	1895.38 ± 152.22	1640.26 ± 238.25	13.46%	<0.0001
SFG PFC R	superior frontal gyrus/ prefrontal cortex (right)	9863.88 ± 807.00	8559.52 ± 1108.31	13.22%	<0.0001
SS L	sagittal stratum (left)	3600.79 ± 425.58	3133.26 ± 369.69	12.98%	0.0005
SFG PFC L	superior frontal gyrus/ prefrontal cortex (left)	10,681.38 ± 932.80	9329.07 ± 1253.48	12.66%	0.0002
SFWM PFC R	subcortical white matter of the superior frontal gyrus/ prefrontal cortex(right)	7427.38 ± 574.21	6564.15 ± 868.70	11.62%	0.0002
CGC L	cingulum (cingulate gyrus part) (left)	2748.25 ± 308.43	2428.85 ± 346.11	11.62%	<0.0001
Cerebellum WM L	cerebellum white matter (left)	8381.50 ± 5870	7422.67 ± 688.66	11.44%	0.0001
Cerebellum WM R	cerebellum white matter (right)	8987.25 ± 720.23	8057.74 ± 705.52	10.34%	0.0003
WD > HC					
SylTempSul L	Sylvian fissure and posterior insular sulcus (left)	2121.67 ± 433.84	2995.89 ± 816.57	-41.20%	<0.0001
SylTempSul R	Sylvian fissure and posterior insular sulcus (right)	1828.75 ± 437.36	2583.85 ± 753.69	-41.29%	<0.0001
SylFrontSul L	Sylvian fissure and anterior insular sulcus (left)	1893.21 ± 451.61	2677.74 ± 904.79	-41.44%	0.0002
III ventricle	third ventricle	1804.25 ± 440.55	3117.70 ± 745.88	-72.80%	<0.0001
Chroid LVetc R	choroid plexus of the lateral ventricle etc. (right)	130.38 ± 44.77	243.48 ± 64.74	-86.75%	<0.0001
Chroid LVetc L	choroid plexus of the lateral ventricle etc. (left)	160.38 ± 55.56	301.74 ± 80.34	-88.14%	<0.0001
LV Frontal R	frontal horn of the lateral ventricle (right)	3073.38 ± 1927.92	7245.26 ± 2993.32	-135.74%	<0.0001
LV Frontal L	frontal horn of the lateral ventricle (left)	3251.38 ± 2434.69	7729.48 ± 3118.25	-137.73%	<0.0001

Data are expressed as mean ± standard deviation and arranged according to the volume decrease rate. All results are significant with FWER correction ($P < 0.05$)

HC Healthy controls; WD Wilson's disease; R right; L left

References

- Aggarwal, A., Aggarwal, N., Nagral, A., Jankharia, G., & Bhatt, M. (2009). A novel global assessment scale for Wilson's disease (GAS for WD). *Movement Disorders*, 24(4), 509–518.
- Ala, A., Walker, A. P., Ashkan, K., Dooley, J. S., & Schilsky, M. L. (2007). Wilson's disease. *LANCET*, 369(9559), 397–408.
- Ashburner, J. (2009). Computational anatomy with the SPM software. *Magnetic Resonance Imaging*, 27(8), 1163–1174.
- Bandmann, O., Weiss, K. H., & Kaler, S. G. (2015). Wilson's disease and other neurological copper disorders. *The Lancet Neurology*, 14(1), 103–113.
- Bostan, A. C., & Strick, P. L. (2018). The basal ganglia and the cerebellum: Nodes in an integrated network. *Nature Reviews Neuroscience*, 19(6), 338–350.
- Caruana, F., Gerbella, M., Avanzini, P., Gozzo, F., Pelliccia, V., Mai, R., Abdollahi, R. O., Cardinale, F., Sartori, I., Lo Russo, G., & Rizzolatti, G. (2018). Motor and emotional behaviours elicited by electrical stimulation of the human cingulate cortex. *Brain*, 141(10), 3035–3051.
- Chen, B., Wang, S., Sun, W., Shang, X., Liu, H., Liu, G., Gao, J., et al. (2017). Functional and structural changes in gray matter of parkinson's disease patients with mild cognitive impairment. *European Journal of Radiology* 93(16-23).
- Członkowska, A., Litwin, T., Dusek, P., Ferenci, P., Lutsenko, S., Medici, V., Rybakowski, J. K., Weiss, K. H., & Schilsky, M. L. (2018). Wilson disease. *Nature Reviews. Disease Primers*, 4(1), 21.
- Dale, A. M., Fischl, B., & Sereno, M. I. (1999). Cortical surface-based analysis. *Neuroimage*, 9(2), 179–194.
- Desikan, R. S., Ségonne, F., Fischl, B., Quinn, B. T., Dickerson, B. C., Blacker, D., Buckner, R. L., Dale, A. M., Maguire, R. P., Hyman, B. T., Albert, M. S., & Killiany, R. J. (2006). An automated labeling system for subdividing the human cerebral cortex on MRI scans into gyral based regions of interest. *Neuroimage*, 31(3), 968–980.
- Ferenci, P., Caca, K., Loudianos, G., Mieli-Vergani, G., Tanner, S., Sternlieb, I., Schilsky, M., Cox, D., & Berr, F. (2003). Diagnosis and phenotypic classification of Wilson disease. *Liver International*, 23(3), 139–142.
- Fischl, B., & Dale, A. M. (2000). Measuring the thickness of the human cerebral cortex from magnetic resonance images. *Proceedings of the National Academy of Sciences*, 97(20), 11050–11055.
- Fischl, B., Sereno, M. I., Tootell, R. B., & Dale, A. M. (1999). High-resolution intersubject averaging and a coordinate system for the cortical surface. *Human Brain Mapping*, 8(4), 272–284.
- Fischl, B., van der Kouwe, A., Destrieux, C., Halgren, E., Segonne, F., Salat, D. H., Busa, E., et al. (2004). Automatically parcellating the human cerebral cortex. *Cerebral Cortex*, 14(1), 11–22.
- Guo, F., Xi, Y., Gao, M., Liu, L., Fei, N., Qin, W., Li, C., et al. (2018). Alterations in cortical thickness in nonmedicated premature ejaculation patients: A morphometric MRI study. *Journal of Magnetic Resonance Imaging*, 47(3), 656–662.
- Hamilton, M. (1959). The assessment of anxiety states by rating. *The British Journal of Medical Psychology*, 32(1), 50–55.
- Hamilton, M. (1960). A rating scale for depression. *J Neurol Neurosurg Psychiatry* 23(56-62).
- Hu, X., Chen, S., Huang, C., Qian, Y., & Yu, Y. (2017). Frequency-dependent changes in the amplitude of low-frequency fluctuations in patients with Wilson's disease: A resting-state fMRI study. *Metabolic Brain Disease*, 32(3), 685–692.
- Jadav, R., Saini, J., Sinha, S., Bagepally, B., Rao, S., & Taly, A. B. (2013). Diffusion tensor imaging (DTI) and its clinical correlates in drug naïve Wilson's disease. *Metabolic Brain Disease*, 28(3), 455–462.
- Kalita, J., Naik, S., Bhoi, S. K., Misra, U. K., Ranjan, A., & Kumar, S. (2017). Pontomesencephalic atrophy and postural instability in Wilson disease. *American Journal of Neuroradiology*, 38(7), 1343–1347.
- Kamagata, K., Zalesky, A., Hatano, T., Ueda, R., Di Biase, M. A., Okuzumi, A., Shimoji, K., et al. (2017). Gray matter abnormalities in idiopathic Parkinson's disease: Evaluation by diffusional kurtosis imaging and Neurite orientation dispersion and density imaging. *Human Brain Mapping*.
- Li, W., Qin, W., Liu, H., Fan, L., Wang, J., Jiang, T., Yu, C. (2013). Subregions of the human superior frontal gyrus and their connections. *Neuroimage* 78(46-58).
- Li, X., Feng, Z., Tang, W., Yu, X., Qian, Y., Liu, B., Li, X., et al. (2018). Sex differences in clinical characteristics and brain MRI change in patients with Wilson's disease in a Chinese population. *Frontiers in Physiology* 9(1429).
- Liu, C. F., Padhy, S., Ramachandran, S., Wang, V. X., Efimov, A., Bernal, A., Shi, L., et al. (2019). Using deep Siamese neural networks for detection of brain asymmetries associated with Alzheimer's disease and mild cognitive impairment. *Magnetic Resonance Imaging* 64(190-199).
- Lorincz, M. T. (2018). Wilson disease and related copper disorders. *Handb Clin Neurol* 147(279-292).
- Mori, S., Wu, D., Ceritoglu, C., Li, Y., Kolasny, A., Vaillant, M. A., Faria, A. V., Oishi, K., & Miller, M. I. (2016). MRICloud: Delivering high-throughput MRI Neuroinformatics as cloud-based software as a service. *Computing in Science & Engineering*, 18(5), 21–35.
- Rodriguez-Castro, K. I. (2015). Wilson's disease: A review of what we have learned. *World Journal of Hepatology*, 7(29), 2859–2870.
- Stezin, A., George, L., Jhunjhunwala, K., Lenka, A., Saini, J., Netravathi, M., Yadav, R., et al. (2016). Exploring cortical atrophy and its clinical and biochemical correlates in Wilson's disease using voxel based morphometry. *Parkinsonism & Related Disorders* 30(52-57).
- Tang, X., Oishi, K., Faria, A. V., Hillis, A. E., Albert, M. S., Mori, S., & Miller, M. I. (2013). Bayesian parameter estimation and segmentation in the multi-atlas random orbit model. *PLoS One*, 8(6), e65591.
- Tang, X., Holland, D., Dale, A. M., Younes, L., & Miller, M. I. (2014). Shape abnormalities of subcortical and ventricular structures in mild cognitive impairment and Alzheimer's disease: Detecting, quantifying, and predicting. *Human Brain Mapping*, 35(8), 3701–3725.
- Tombaugh, T. N., & McIntyre, N. J. (1992). The mini-mental state examination: A comprehensive review. *Journal of the American Geriatrics Society*, 40(9), 922–935.
- Wang, H., Pouch, A., Takabe, M., Jackson, B., Gorman, J., Gorman, R., Yushkevich, P. A. (2013). Multi-atlas segmentation with robust label transfer and label fusion. *Inf Process Med Imaging* 23(548-559).
- Zhang, Y., Zhou, W., Wang, S., Zhou, Q., Wang, H., Zhang, B., Huang, J., Hong, B., & Wang, X. (2019). The roles of subdivisions of human insula in emotion perception and auditory processing. *Cerebral Cortex*, 29(2), 517–528.
- Zou, L., Song, Y., Zhou, X., Chu, J., & Tang, X. (2019). Regional morphometric abnormalities and clinical relevance in Wilson's disease. *Movement Disorders*, 34(4), 545–554.

Publisher's note Springer Nature remains neutral with regard to jurisdictional claims in published maps and institutional affiliations.